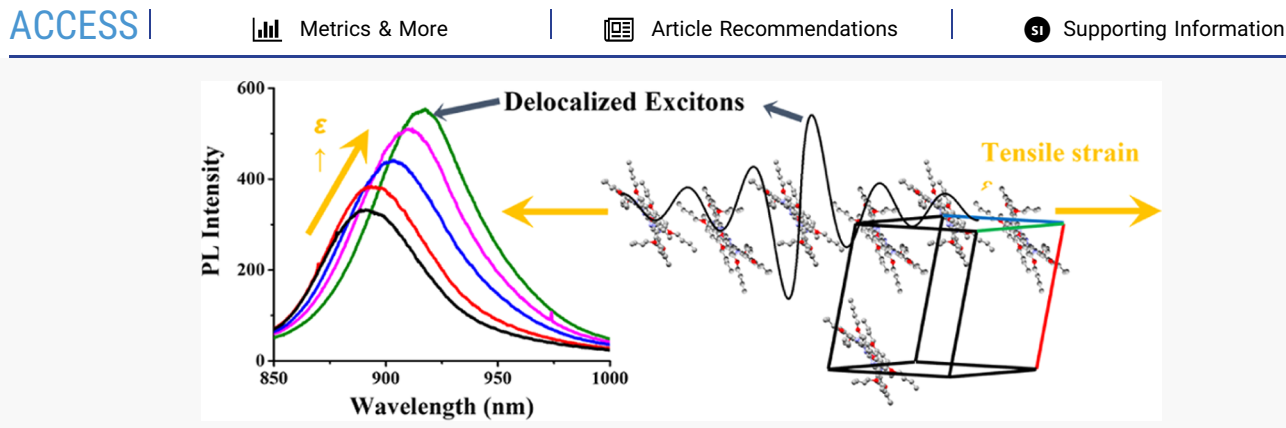


pubs.acs.org/JPCC Article

# Strain-Enhanced Formation of Delocalized Exciton States in Phthalocyanine Crystalline Thin Films

Libin Liang, Katrina Czar, and Madalina I. Furis\*





ABSTRACT: The formation of delocalized excitonic states in organic semiconductors is highly desirable because it leads to efficient energy transport in devices. We investigate the potential of uniaxial strain as a "tuning dial" for delocalized excitons (i.e., exciton—polarons) in crystalline thin films of soluble octabutoxy phthalocyanine. Absorption and photoluminescence spectra confirm the formation of delocalized excitonic states in the presence of tensile strain, accompanied by a red shift of low-frequency vibration modes (<100 cm<sup>-1</sup>) in Raman spectroscopy, which are likely responsible for the delocalized exciton formation. Remarkably, an 80% enhancement in photoluminescence intensity and a 30 nm red shift in peak wavelength are observed for a tensile strain of 4.9%, which is equivalent to a temperature reduction approximately by 100 K below room temperature. These results show promise that strain engineering can efficiently modify the exciton—phonon coupling in octabutoxy phthalocyanine crystalline thin films toward enabling delocalization at room temperature.

# **■ INTRODUCTION**

Organic semiconductors are well-known candidates for flexible, wearable, and portable novel electronic and photonic devices <sup>1-3</sup> because of their tunable optoelectronic properties, versatile synthetic pathways, and desirable mechanical properties. <sup>4,5</sup> More recently, the advent of new thin-film fabrication techniques <sup>6-8</sup> in conjunction with sustained efforts to gain more insight into the structure—property relationships of these materials stimulated an increasing number of researchers to explore small-molecule semiconductors as possible platforms for robust coherent excitonic states, <sup>9-13</sup> topological states, <sup>14-17</sup> and quantum applications. <sup>18,19</sup>

In this context, externally applied mechanical strain emerges as an effective candidate for tuning organic semiconductor device properties.<sup>20–24</sup> Historically, electronic and excitonic properties of inorganic semiconductor devices could be tuned by applying a small strain.<sup>7,25–30</sup> For example, it is well established that in a 2D transition metal dichalcogenides system, a strain of <1.6% can significantly affect exciton energy, modify electron—phonon coupling, lift the degeneracy of lattice vibration modes, and tune direct/indirect band gap.<sup>30–33</sup> In low-dimensional small-molecule semiconductors,

the nature of excitonic states is radically different from the 2D chalcogenides or inorganic semiconductors in general; <sup>34,35</sup> therefore, the possible effects of strain on the already complex many-body picture of exciton formation are not fully understood. Generally, the strain could affect the equilibrium position of molecules in a crystal lattice, <sup>7</sup> resulting in the change of charge carrier mobilities and excitonic coupling due to the change in average transfer integrals <sup>36</sup> and wavefunction overlap between nearest neighbors. <sup>37</sup> Strain could also affect inter-<sup>20</sup> and intramolecular <sup>21,24</sup> vibrations, which are responsible for charge carrier band-like transport <sup>38–40</sup> and exciton coherence regime. <sup>37,41–43</sup> In laboratories, strain is conventionally introduced to organic systems with a bending approach, <sup>20,28,30,32</sup> which would enable one to perform compressive or tensile strain-dependent studies simultane-

Received: February 25, 2022 Revised: April 26, 2022 Published: May 11, 2022





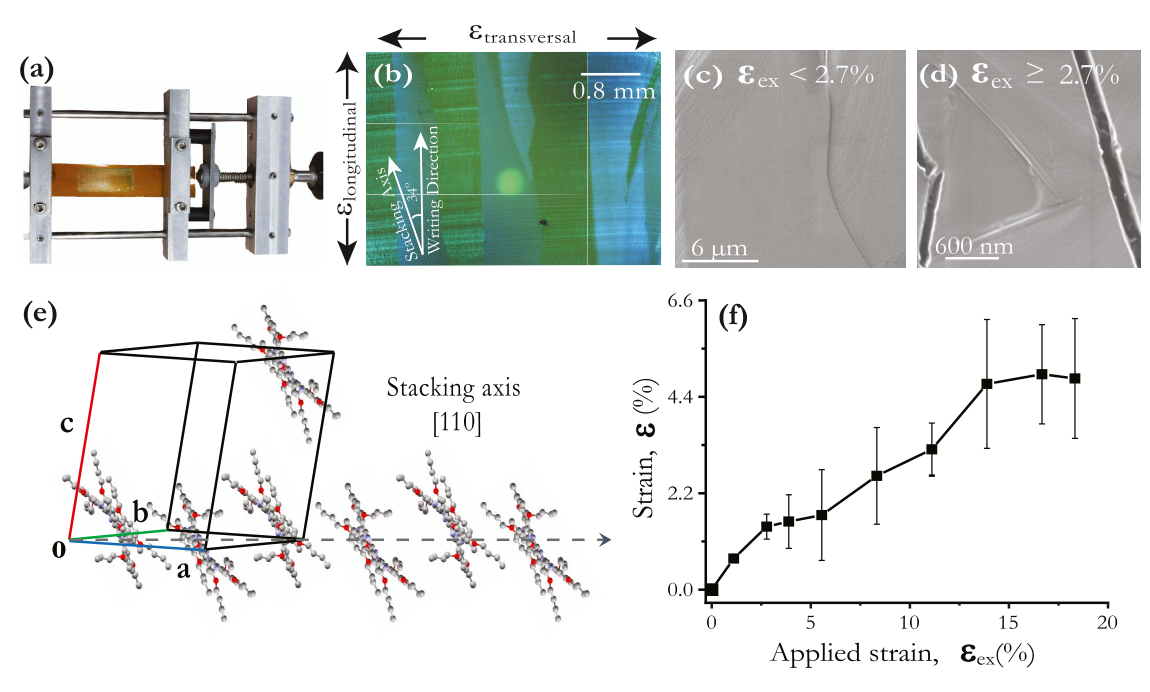


Figure 1.  $H_2$ -OBPc thin film on flexible Kapton substrates under strain. (a) Photograph of an  $H_2$ -OBPc thin film deposited on a 5 cm  $\times$  1 cm Kapton substrate, mounted on a home-built stretching device. (b) In situ polarized telescope image of the same  $H_2$ -OBPc thin film subjected to tensile strain. The bright green disk is the quasi-monochromatic focused beam used in the absorbance experiment. The orientation of the longitudinal and transversal applied strain is shown in relation to the pen-writing direction. (c) SEM image of the thin-film surface remains smooth for applied strains lower than 2.7%. (d) SEM image of the thin-film surface recorder for large, applied strain reveals the formation of cracks (e)  $H_2$ -OBPc molecular stacking in the crystalline phase rendered from X-ray diffraction measurements by Gao et al. (f) Evolution of the effective strain experienced by the thin film as a function of the longitudinal applied strain experienced by the Kapton substrate. The procedure for obtaining the effective strain values is described in detail in the SI.

ously, with little defects introduced, and quantify the strain value from the bending geometry and the thin-film thickness. However, this method is less suited for optical and excitonic properties quantitative measurements, especially if they involve precise excitation beam size and position control. For example, there are no reported observations of strain-induced enhancement of photoluminescence intensity in previous studies. Alternatively, as proposed in the presented work, uniaxial stretching would be a promising approach for quantitative analysis of strain-dependent optical and excitonic properties, provided defects introduced to the thin films are carefully monitored and characterized. Furthermore, this experimental approach can be easily adapted to a cryogenic environment for temperature-dependent studies.

In the presented work, we explore the effects of uniaxial strain on 1D exciton coherence in  $H_2$ -OBPc thin films with macroscopic grain sizes, deposited on flexible Kapton substrates. Octabutoxy phthalocyanine ( $H_2$ -OBPc) is a soluble derivative of the phthalocyanines (Pc's) that exhibits 1D coherent excitons as previous experimental  $^{42,45-47}$  and theoretical  $^{37,41}$  studies suggest, a result of the interplay between three energy scales: short-range  $\pi$ - $\pi$  stacking, longrange Coulomb forces, exciton—lattice/molecular vibration couplings. Our recent study of coherent exciton—polaron formation in these molecules  $^{47}$  implies a possibility to tune coherent exciton properties at room temperature with applied strain. However, a direct relationship between the excitonic property, the molecular vibrations, and external applied mechanical strain has not been experimentally established yet.

# **■** METHODS

**Thin-Film Preparation.** 1,4,8,11,15,18,22,25-Octabutoxy-29H,31H-phthalocyanine ( $H_2$ -OBPc) from Sigma-Aldrich was used to prepare thin films on a flexible Kapton substrate from Dupont (75  $\mu$ m in thickness, Poisson ratio p=0.34, ultraviolet ozone treated for 0.5 h) with a pen-writing technique <sup>6,8</sup> with a 0.5% solution at a writing speed of 17  $\mu$ m/s. More information can be found in refs 42, 45, and 47.

**Absorption Measurement.** Absorption measurements were conducted using the setup in ref 47 with the sample mounted on a stretching device (Figure 1a). The location of the quasi-monochromatic tunable incoherent light beam ( $\sim$ 50  $\mu$ m in diameter) on the sample was monitored in situ using a long-distance telescope. Linear dichroism (LD) was measured with the same setup and is defined as the difference between absorbance measured for two orthogonally polarized light beams: LD =  $A_x - A_y$ .

Diffraction-Limited Photoluminescence (PL) Measurement. Diffraction-limited PL spectra were recorded with a 2300 Princeton Instruments spectrometer coupled to a CCD camera using a 735 nm narrow-band pulsed 200 ps laser excitation. The 90  $\mu$ W laser beam was focused to a 5  $\mu$ m spot on the sample, yielding a power density of 4.6  $\mu$ W/ $\mu$ m². Substrates were mounted on a stretching device designed inhouse (Figure 1a). The location of the excitation beam onto the sample was monitored in situ using a long-distance telescope. The in-plane rotation angle of the emission  $\varphi$  is computed from the photoluminescence polarization P using the x- and y-polarized in-plane components of the PL ( $I_x$  and  $I_y$ ),  $P = (I_x - I_y)/(I_x + I_y) = \cos 2\varphi$ .

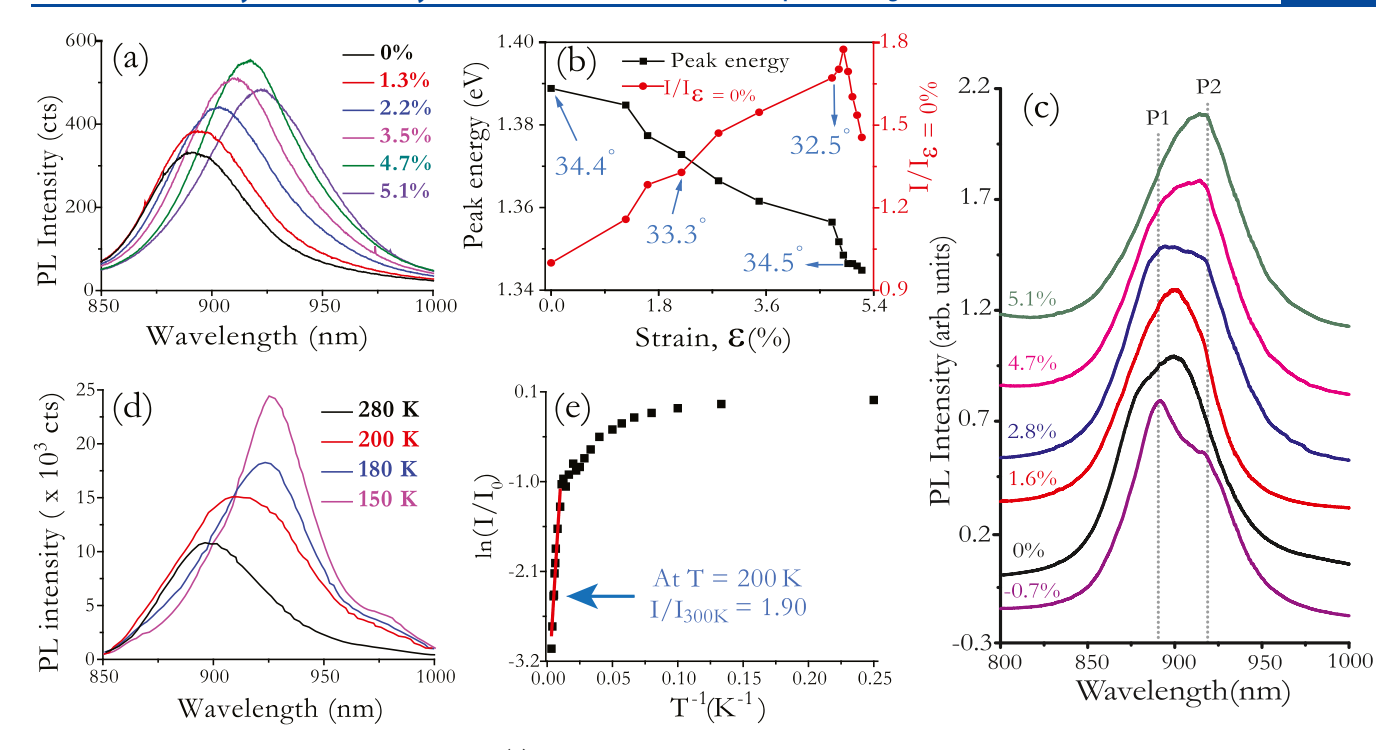


Figure 2. PL measurement of  $H_2$ -OBPc thin films. (a) Evolution of diffraction-limited PL spectra recorded for different applied longitudinal strain values. (b) Longitudinal strain dependence of diffraction-limited PL intensity and peak energy. The angles indicate the polarization of the emission with respect to the vertical direction. (c) Strain-dependent confocal PL spectra recorded for different values of applied strain. The positive values correspond to the longitudinal tensile strain, while the negative values indicate compressive longitudinal (tensile transversal) strain. (d) Temperature-dependent diffraction-limited PL spectra\*. (e) Arrhenius plot of the PL emission intensity evolution with increasing temperature in strain-free  $H_2$ -OBPc thin films\*.

Confocal Raman and PL Measurements. Raman measurements were conducted with a HORIBA LabRam HR Evolution microscope with an incident laser of wavelength 532 nm, a grating of 1800, and an objective of 100x. An ultralowfrequency filter was employed to allow accurate Raman frequencies as low as 25 cm<sup>-1</sup>. Substrates were coated with a Pt/Au (60/40) layer to block any luminescence and Raman signal from Kapton. To avoid sample heating, each Raman spectrum was acquired by averaging the Raman signal recorded from 10 randomly selected locations within the same 5  $\mu$ m × 5 µm area. Confocal PL spectra measurements were conducted over an area of 5  $\mu$ m  $\times$  5  $\mu$ m (9 points by 9 points) with an incident laser of wavelength 785 nm, a grating of 600 gr/mm, and an objective of 100×. For both experiments, the incident laser power was kept below 15  $\mu$ W and the spatial resolution was estimated to be 1  $\mu$ m, yielding the power density of 19.1  $\mu W/\mu m^2$ . PL scanning measurements were conducted within a single spectral acquisition window (874-922 nm) to further avoid sample heating, resulting from long exposure to the laser

**SEM Measurement.** Morphology of a thin-film surface was observed with a Zeiss Sigma 300 VP FE-SEM using an electron beam of 1 keV with a secondary electron detector. To avoid charge accumulation on a nonconductive thin-film surface, the thin film was deposited on Kapton substrates coated with a Pt/Au (60/40) layer. Figure 1c,d shows two examples of the SEM images recorded for different values of the uniaxial strain applied using the stretching device shown in Figure 1a.

# ■ RESULTS AND DISCUSSION

Challenges of Optical Probing in the Presence of Mechanical Strain. Figure 1a shows the in-house built

stretching device employed for the application of an external uniaxial strain  $\varepsilon_{\rm ex}$ . The crystalline thin film with large grain sizes ( $\sim$ mm range) enables the usage of multiple diffraction-limited techniques to study the intrinsic material properties within a single grain. Figure 1b shows an in situ real-time photograph of the quasi-monochromatic focused beam spot used in absorption measurements.

As previous research indicates, H2-OBPc molecules are standing "edge-on" the substrate to form quasi one-dimension chains along the [110] direction (Figure 1e) with molecular stacking axes making a 34° angle with the writing direction. 42,45,47 While intermolecular interaction along the stacking axis 37,42 is quite strong, the interchain interaction is negligible by comparison. 42,48 Therefore, molecular chains can be viewed as a one-dimensional system mainly experiencing tensile strain (positive value)/compressive strain (negative value) in the longitudinal/transversal geometry, as shown in Figure 1b. The crack formation was only observed for applied strain  $\varepsilon_{\rm ex} \geq 2.7\%$  in both longitudinal and transversal geometries, as revealed in SEM microscopy images shown in Figure 1c,d. Partial strain relaxation is expected as a result of defect formation. For this reason, a protocol that includes SEM measurements of crack defects was developed to obtain a realistic estimate of the strain experienced by the organic thin film. Figure 1f shows the relation between the strain along molecular chain  $\varepsilon$  and  $\varepsilon_{ex}$  after the strain correction was performed, as discussed in Supporting Information S1 and S2. For the rest of the paper, we will refer to these corrected  $\varepsilon$ values as the applied strain. Moreover, the application of a transversal tensile strain will generate compressive longitudinal strain along the stacking molecular axis. This will be indicated by negative values of  $\varepsilon$ .

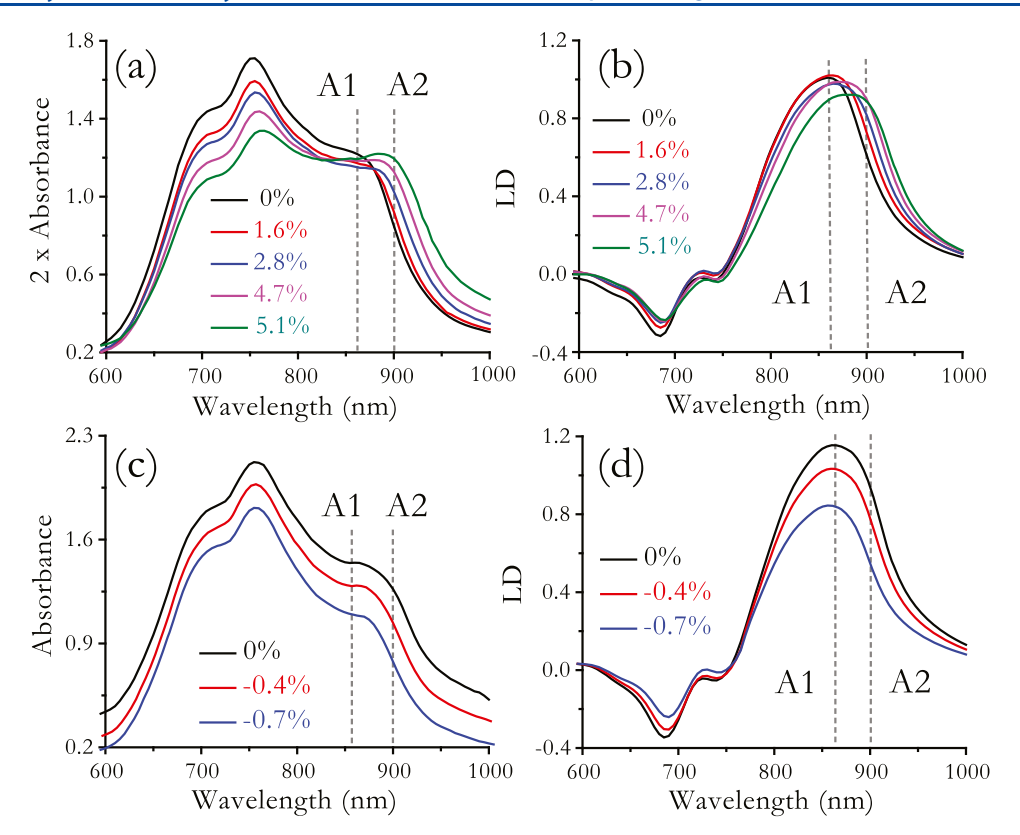


Figure 3. Strain-dependent absorption measurement of the H<sub>2</sub>-OBPc thin film. (a) and (b) Absorption and LD spectra measured for different values of the applied tensile strain. (c) and (d) Absorption and LD spectra measured for different values of the compressive strain.

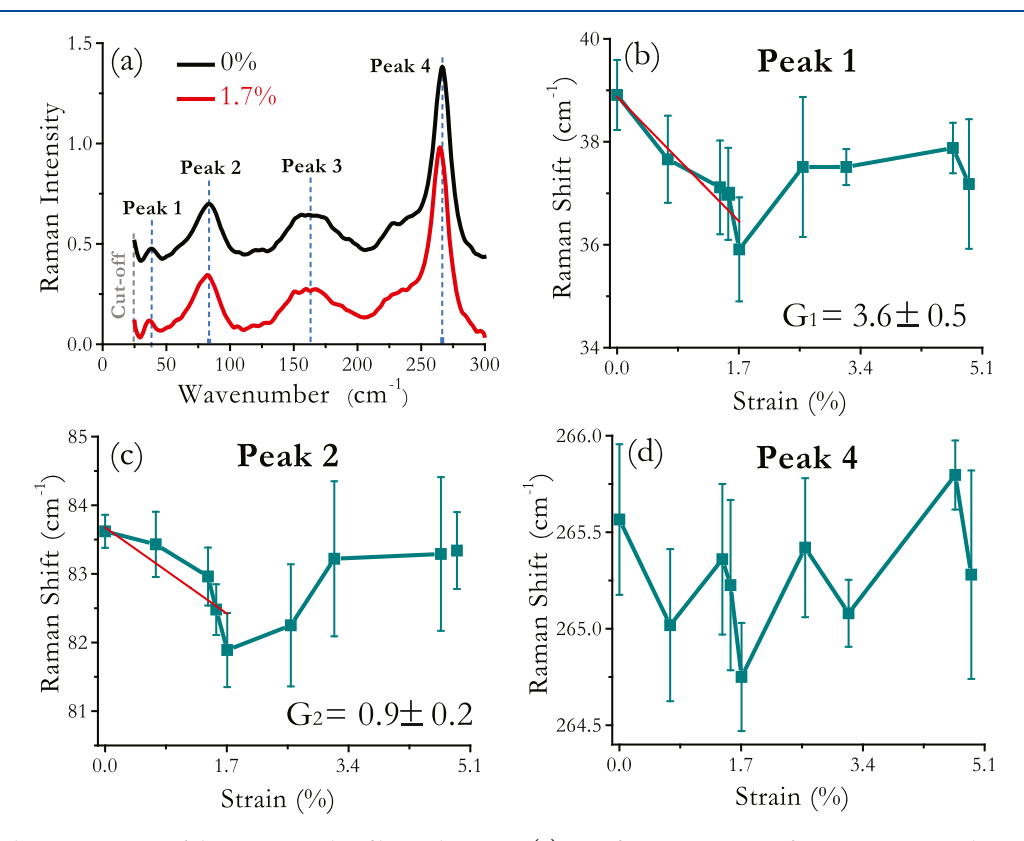


Figure 4. Confocal Raman spectra of the  $H_2$ -OBPc thin film under strain. (a) Low-frequency region of Raman spectra with resolved peaks 1, 2, 4 and a broad peak 3. The instrument cutoff is at  $\approx 25$  cm<sup>-1</sup>. (b)-(d) Evolution of Raman peaks 1, 2, and 4 as a function of longitudinal strain, respectively. The solid red line is a linear fit.

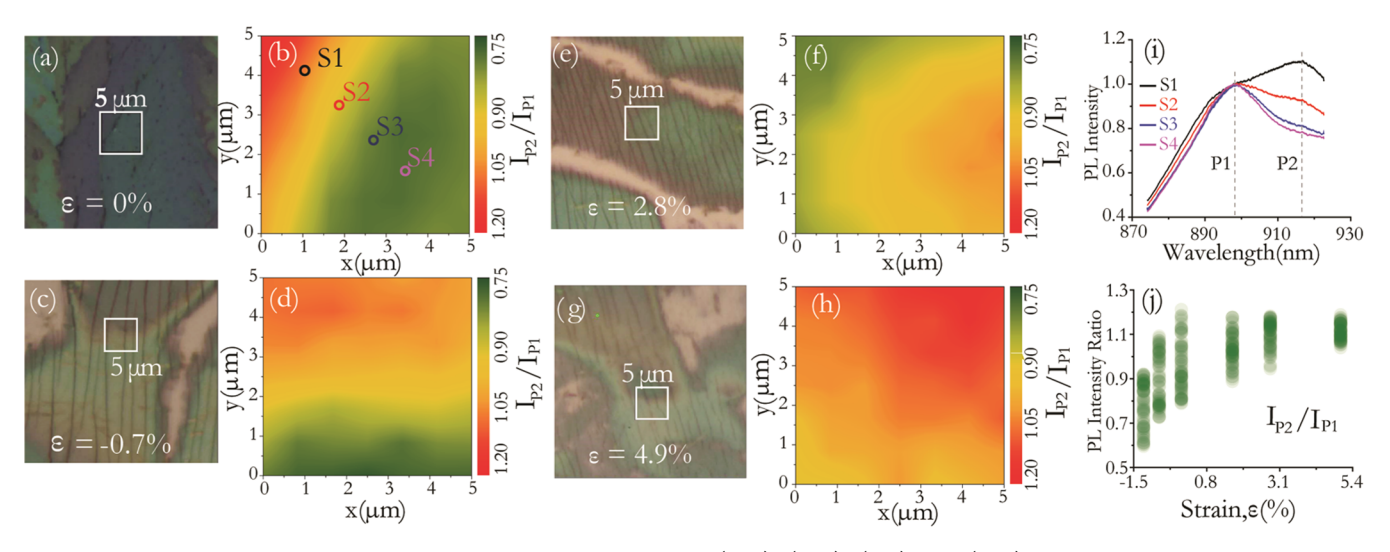


Figure 5. Confocal PL scanning microscopy of the H<sub>2</sub>-OBPc thin film. (a, b), (c, d), (e, f), and (g, h) In situ microscopy images and the corresponding contour plot of  $I_{P2}/I_{P1}$  of a 5 × 5 μm<sup>2</sup> area, under strain  $\varepsilon$  = 0, -0.7, 8, and 4.9%, respectively. (i) PL spectra recorded at specific positions (marked S1 through S4) with  $\varepsilon$  = 0%. Spectra were normalized to P1 intensity  $I_{P1}$ . (j) Plot of  $I_{P2}/I_{P1}$  as a function of strain  $\varepsilon$ , each data point represents a different location within the 5 × 5 μm<sup>2</sup> areas, similar to those in (a, c, e, g). A total of 80 locations were sampled for each value of  $\varepsilon$ .

### Strain-Enhanced Formation of Delocalized Excitons.

Figure 2a shows that with increasing strain  $\varepsilon \leq 4.7\%$ , PL intensity increases relative to the one measured in the nominal strain-free film. At the same time, the peak energy red shifts from 1.390 eV (892 nm) to 1.345 eV (922 nm). Figure 2b summarizes these evolutions, indicating that the maximum PL intensity enhancement  $(I/I_{\varepsilon=0\%})|_{\max}$  of 1.8 corresponds to an applied strain of  $\varepsilon$  = 4.9%. Confocal PL spectra recorded for different values of the applied strain (Figure 2c) show that the overall red shift is in fact due to the presence of an additional emission peak at 920 nm (P2), which increases in intensity with increasing strain, relative to the 890 nm emission peak observed in the strain-free condition (P1). Previous temperature studies 42,47 on nominally strain-free H2-OBPc report similar spectral evolution patterns with decreasing temperatures (Figure 2d) due to the delocalized exciton formation. This formation is typically accompanied by a  $5^{\circ}$ rotation in the PL polarization, while a similar 2° rotation is observed in presented work (Figure 2b). More importantly, the spectroscopic signatures of delocalized excitons typically disappear around 175 K. Therefore, we hypothesize that strain enhances the formation of delocalized excitons at room temperature, producing an effect equivalent to that of decreasing sample temperature. We find that at T = 200 K,  $(I/I_{300 \text{ K}})$  yields a similar value (Figure 2e, 1.90) with  $(I/I_{300 \text{ K}})$  $I_{\varepsilon=0\%}|_{\mathrm{max}}$ . That is, the effect of strain on the PL intensity is equivalent to a temperature reduction by approximately 100 K below room temperature. This is a remarkable observation that opens an avenue to the practical use of 1D coherence in a functional device.

Corresponding absorption spectra measured from the strained films also develop an additional absorption peak at 900 nm (A2 in Figure 3a), polarized similarly to the 865 nm band-gap absorption feature of the unstrained film (large linear dichroism in Figure 3b). In contrast, for compressive strain values of  $\varepsilon \leq -0.7\%$ , the P2 intensity decreases and P1 is, therefore, better resolved. The relevant absorption spectra show that A2 decreases (Figure 3c) and the LD spectra exhibit a small blue shift of the main peak (Figure 3d).

The PL intensity, peak energy, and absorbance spectra trend with increasing strain change significantly for tensile strain values of  $\varepsilon > 4.7\%$ . They exhibit an overall intensity decrease and no changes in the peak energies (Figure 2b). A similar pattern is also observed with increasing compressive  $\varepsilon$  (Figure 3c,d). Such a decrease is most likely associated with the fact that less material is being excited by the focused beam as larger densities of cracks develop with large strain, in agreement with Figure 1c. Therefore, the excitonic states are no longer affected by the applied strain for  $\varepsilon > 4.7\%$ .

Effect of Strain on Vibration Modes. A previous theoretical study<sup>37</sup> on H<sub>2</sub>-OBPc suggests that the low-energy vibration modes (below 100 cm<sup>-1</sup> and approx. 300 cm<sup>-1</sup> control the intermolecular excitonic coupling and are thus critical ingredients for the formation of delocalized excitonpolaron states. The similarity between the end results of lowering temperature and applying strain demands further exploration of the vibration modes and their coupling to excitons. To this end, we performed measurements of lowfrequency Raman spectra of flexible crystalline H2-OBPc thin films as a function of the applied uniaxial strain. Figure 4a shows the typical Raman spectra with/without strain, exhibiting three clearly resolved peaks (labeled as peaks 1, 2, and 4) and a broader peak 3. Previous Raman studies<sup>49–52</sup> suggest that the 265.5 cm<sup>-1</sup> vibration mode (peak 4) is associated with the isoindole molecular breathing mode. Lowenergy vibration modes below 200 cm<sup>-1</sup> are rarely reported and are generally considered to be determined by crystal symmetry and correspond to the lattice vibrations<sup>49</sup> (i.e., phonon modes). The strain-dependent evolution of the Raman peaks 1, 2, and 4 is shown in Figure 4b-d. Measurement results show that 39 and 83.5 cm<sup>-1</sup> low-energy vibration modes (peak 1 and 2, respectively) shift to lower frequencies for a tensile strain of  $\varepsilon \leq 1.7\%$ . Previous studies indicate that the interaction between the molecules strengthens as the nearest neighbor (NN) spacing decreases with compressive strain.<sup>53</sup> Therefore, these red-shifted low-energy Raman peaks are indicative of the softening of the corresponding phonon modes of the crystal with tensile strain (larger vibration

amplitude). <sup>20</sup> For  $\varepsilon > 1.7\%$ , the vibration modes shift back to higher frequencies and stabilize at frequencies smaller than the unstrained ones, which implies strain relaxation due to crack defects in thin films. Note that the strain relaxation occurs at a lower applied strain level in confocal Raman measurement (1.7%) than that in diffraction-limited PL measurement (4.7%). Most likely, this is the result of a higher energy density of the confocal laser beam on the sample compared with that in diffraction-limited PL, which leads to local sample heating and consequently to strain relaxation.

The effect of strain on the frequency of Raman modes can be quantified by the Grüneisen parameter G, which is the fractional change of vibration frequency  $(\partial f/f)$  per fractional change of sample volume  $(\partial V/V)$ . <sup>54</sup> In present work with uniaxial strain, the  $\partial V/V$  is equivalent to the fractional change in linear dimension (i.e.,  $\partial l/l$ ) (negligible interchain interaction). Therefore, the parameter G for a given Raman mode could be expressed in terms of  $\varepsilon$ , as Choi et al.<sup>20</sup> suggest:  $G_i \equiv -\frac{1}{f_i} \cdot \frac{\partial f_i}{\partial e}$ . Calculation results show that the low-energy vibration modes are sensitive to strain, and the 39 cm<sup>-1</sup> vibration mode is more affected by strain than the 83.5 cm<sup>-1</sup> vibration mode (G1 being larger than G2, as shown in Figure 4b,c). In contrast, the 265.5 cm<sup>-1</sup> vibration mode exhibits no clear trend versus strain  $\varepsilon$ . For Raman modes with a greater frequency than 265.5 cm<sup>-1</sup>, no obvious frequency shift is observed with/without strain (Supporting Information S3), a behavior expected for localized molecular vibrations. By analyzing the relation between PL intensity and Raman frequency with the same temperature variation (Supporting Information S4), we find that to achieve the same fractional change of PL intensity, tuning the low-energy Raman vibration frequency is twice more effective than tuning the sample temperature. As mentioned earlier, the enhancement in PL intensity is due to the formation of delocalized excitonpolaron states. Therefore, tuning strain can be an effective and more practical means to enhance the exciton delocalization when compared to lowering film temperature.

Effect of Residual Strain on the Formation of **Delocalized Excitons.** Previous studies indicated<sup>7,55</sup> that residual stress could be generated in the thin film during the crystallization process, which could, in turn, affect the lattice spacing. We investigated whether the apparent thin-film nonuniformities observed with an optical microscope (Figure 5a) are related to the presence of residual strain inhomogeneities, which could impact the excitonic properties of a nominally strain-free film. A confocal PL scanning measurement was performed over a 5  $\mu$ m  $\times$  5  $\mu$ m area that exhibits some color contrast in the unstretched thin film (Figure 5a), imaging the intensity ratio between the two excitonic peaks  $I_{\rm P2}/I_{\rm P1}$  (Figure 5b). A corresponding mapping relationship was obtained between the image acquired under a confocal optical microscope and the scanning plot, with a clear color contrast for the regions where we observe apparent nonuniformities. Similar results are observed with compressive strain (Figure 5c,d for -0.7%) and tensile strain (Figure 5e,f for 2.8% and Figure 5g,h for 4.9%); however, the range of the  $I_{P2}/I_{P1}$  values over the scanned areas decreases significantly with increasing strain as reflected by the decreasing contrast in the figures. To better quantify this effect, the photoluminescence spectrum was sampled at 80 randomly selected locations across the film. Four of these spectra, recorded at locations labeled S1 through S4, are presented in Figure 5i. The intensity is normalized with

respect to the value recorded for the peak P1. By comparing the four spectra, we can clearly see that the coherent excitons (peak P2) dominate the spectrum recorded from certain locations such as S1, indicating there is some residual amount of strain prior to stretching. The statistics of the intensity ratio  $I_{\rm P2}/I_{\rm P1}$ , presented in Figure 5j, indicated that the range of values for this ratio decreases significantly in the presence of externally applied uniaxial strain. This result implies that the introduction of the external uniaxial strain minimizes strain fluctuations that lead to fluctuations in the relative intensity of the two peaks prior to stretching. That is, randomly distributed built-in residual strain exists in the thin film, favoring the delocalized exciton state formation at random locations; the strain distribution in the thin film becomes more uniform with increasing external applied strain and the formation of delocalized excitons extends over the entire film. These results could further explain the large standard deviation of the vibration frequency observed in the confocal Raman measurement (Figure 4). Also, they imply that introducing and controlling built-in strain during the deposition process could be beneficial for delocalized exciton formation. For example, it opens a new avenue to tune the electronic and excitonic properties of phthalocyanine-based and solution-processable semiconductor devices with a well-defined molecular crystal structure.56-58

#### CONCLUSIONS

In conclusion, strain-enhanced delocalized exciton states were observed in crystalline H2-OBPc thin films at room temperature. We find that the uniaxial tensile strain can soften the lattice vibration modes and increase PL intensity up to 1.8-fold with delocalized band-gap transitions at longer wavelengths. The tensile strain strengthens the delocalized states, its effect being equivalent to the lowering of temperature by 100 K.

We also find that the built-in strain that develops in the thin films during deposition can be sufficient to impact the excitonic properties. These observations support a view of the large tunability of excitonic states under tensile strain as a promising tool to overcome the fundamental limits of the carrier and exciton mobility imposed by the molecular architecture and thermal fluctuations. Our results also inform future evolution of solution-based deposition methods and efforts to improve thin-film uniformity. Last but not least, the strain-dependent experiments can point synthetic and quantum chemists toward the ideal stacking geometry required for a room temperature coherent excitons device.

# ASSOCIATED CONTENT

# **Solution** Supporting Information

The Supporting Information is available free of charge at https://pubs.acs.org/doi/10.1021/acs.jpcc.2c01382.

Strain correction approach, confocal Raman spectral under strain at a high-frequency region, and derivation of the relationship between PL intensity, vibration mode, and strain  $\varepsilon$  (PDF)

# AUTHOR INFORMATION

#### **Corresponding Author**

Madalina I. Furis – Homer L. Dodge Physics Department, University of Oklahoma, Norman, Oklahoma 73019, United States; Materials Science Program and Department of Physics, University of Vermont, Burlington, Vermont 05405, *United States;* orcid.org/0000-0001-9007-5492; Phone: (405) 934 2221; Email: madalina.furis@ou.edu

#### **Authors**

Libin Liang – Materials Science Program and Department of Physics, University of Vermont, Burlington, Vermont 05405, United States

Katrina Czar – Systems Architecture & Admin and Department of Physics, University of Vermont, Burlington, Vermont 05405, United States

Complete contact information is available at: https://pubs.acs.org/10.1021/acs.jpcc.2c01382

#### Notes

The authors declare no competing financial interest.

# ACKNOWLEDGMENTS

This material is based upon work supported by the National Science Foundation under Grant numbers: DMR-1056589, DMR-1919610, DMR-0821268, and DMR-1828371 and the University of Vermont Sustainable Campus Fund. The authors especially thank UVM physics instrument shop technician Douglas Gomez for the machining of the sample holder used in strain-dependent absorption and photoluminescence experiments.

#### REFERENCES

- (1) Martínez-Díaz, M. V.; de la Torre, G.; Torres, T. Lighting Porphyrins and Phthalocyanines for Molecular Photovoltaics. *Chem. Commun.* **2010**, *46*, 7090–7108.
- (2) Walter, M. G.; Rudine, A. B.; Wamser, C. C. Porphyrins and Phthalocyanines in Solar Photovoltaic Cells. *J. Porphyrins Phthalocyanines* **2010**, *14*, 759–792.
- (3) Uoyama, H.; Goushi, K.; Shizu, K.; Nomura, H.; Adachi, C. Highly Efficient Organic Light-Emitting Diodes from Delayed Fluorescence. *Nature* **2012**, *492*, 234–238.
- (4) Ostroverkhova, O. Organic Optoelectronic Materials: Mechanisms and Applications. *Chem. Rev.* **2016**, *116*, 13279–13412.
- (5) Chidichimo, G.; Filippelli, L. Organic Solar Cells: Problems and Perspectives. *Int. J. Photoenergy* **2010**, 2010, 1–11.
- (6) Wo, S.; Headrick, R. L.; Anthony, J. E. Fabrication and Characterization of Controllable Grain Boundary Arrays in Solution-Processed Small Molecule Organic Semiconductor Films. *J. Appl. Phys.* **2012**, *111*, No. 073716.
- (7) Giri, G.; Verploegen, E.; Mannsfeld, S. C.; Atahan-Evrenk, S.; Kim, D. H.; Lee, S. Y.; Becerril, H. A.; Aspuru-Guzik, A.; Toney, M. F.; Bao, Z. Tuning Charge Transport in Solution-Sheared Organic Semiconductors Using Lattice Strain. *Nature* **2011**, *480*, 504–508.
- (8) Headrick, R. L.; Wo, S.; Sansoz, F.; Anthony, J. Anisotropic Mobility in Large Grain Size Solution Processed Organic Semi-conductor Thin Films. *Appl. Phys. Lett.* **2008**, *92*, No. 063302.
- (9) Najafov, H.; Lee, B.; Zhou, Q.; Feldman, L. C.; Podzorov, V. Observation of Long-Range Exciton Diffusion in Highly Ordered Organic Semiconductors. *Nat. Mater.* **2010**, *9*, 938–943.
- (10) Vagenas, N.; Podzorov, V.; Kounavis, P. Modulated-Photocurrent Spectroscopy of Single-Crystal Organic Semiconductor Rubrene with Pristine and Trap-Dominated Surfaces. *Phys. Rev. Mater.* **2021**, *5*, No. 063801.
- (11) Nelson, T. R.; Ondarse-Alvarez, D.; Oldani, N.; Rodriguez-Hernandez, B.; Alfonso-Hernandez, L.; Galindo, J. F.; Kleiman, V. D.; Fernandez-Alberti, S.; Roitberg, A. E.; Tretiak, S. Coherent Exciton-Vibrational Dynamics and Energy Transfer in Conjugated Organics. *Nat. Commun.* **2018**, *9*, No. 2316.
- (12) Valleau, S.; Saikin, S. K.; Yung, M.-H.; Guzik, A. A. Exciton Transport in Thin-Film Cyanine Dye J-Aggregates. *J. Chem. Phys.* **2012**, *137*, No. 034109.

- (13) Hou, S.; Khatoniar, M.; Ding, K.; Qu, Y.; Napolov, A.; Menon, V. M.; Forrest, S. R. Ultralong-Range Energy Transport in a Disordered Organic Semiconductor at Room Temperature Via Coherent Exciton-Polariton Propagation. *Adv. Mater.* **2020**, 32, No. 2002127
- (14) Yuen-Zhou, J.; Saikin, S. K.; Yao, N. Y.; Aspuru-Guzik, A. Topologically Protected Excitons in Porphyrin Thin Films. *Nat. Mater.* **2014**, *13*, 1026–1032.
- (15) Yuen-Zhou, J.; Saikin, S. K.; Zhu, T.; Onbasli, M. C.; Ross, C. A.; Bulovic, V.; Baldo, M. A. Plexciton Dirac Points and Topological Modes. *Nat. Commun.* **2016**, *7*, No. 11783.
- (16) Jiang, W.; Zhang, S.; Wang, Z.; Liu, F.; Low, T. Topological Band Engineering of Lieb Lattice in Phthalocyanine-Based Metal—Organic Frameworks. *Nano Lett.* **2020**, 20, 1959—1966.
- (17) Leisegang, M.; Christ, A.; Haldar, S.; Heinze, S.; Bode, M. Molecular Chains: Arranging and Programming Logic Gates. *Nano Lett.* **2021**, *21*, 550–555.
- (18) Cheung, D. L.; Troisi, A. Modelling Charge Transport in Organic Semiconductors: From Quantum Dynamics to Soft Matter. *Phys. Chem. Chem. Phys.* **2008**, *10*, 5941–5952.
- (19) Fratini, S.; Mayou, D.; Ciuchi, S. The Transient Localization Scenario for Charge Transport in Crystalline Organic Materials. *Adv. Funct. Mater.* **2016**, *26*, 2292–2315.
- (20) Choi, H. H.; Yi, H. T.; Tsurumi, J.; Kim, J. J.; Briseno, A. L.; Watanabe, S.; Takeya, J.; Cho, K.; Podzorov, V. A Large Anisotropic Enhancement of the Charge Carrier Mobility of Flexible Organic Transistors with Strain: A Hall Effect and Raman Study. *Adv. Sci.* **2020**, *7*, No. 1901824.
- (21) Ruggiero, M. T.; Ciuchi, S.; Fratini, S.; D'avino, G. Electronic Structure, Electron-Phonon Coupling, and Charge Transport in Crystalline Rubrene under Mechanical Strain. *J. Phys. Chem. C* **2019**, 123, 15897—15907.
- (22) Wang, H.; Deng, L.; Tang, Q.; Tong, Y.; Liu, Y. Flexible Organic Single-Crystal Field-Effect Transistor for Ultra-Sensitivity Strain Sensing. *IEEE Electron Device Lett.* **2017**, *38*, 1598–1601.
- (23) Qin, J.; Lan, L.; Chen, S.; Huang, F.; Shi, H.; Chen, W.; Xia, H.; Sun, K.; Yang, C. Recent Progress in Flexible and Stretchable Organic Solar Cells. *Adv. Funct. Mater.* **2020**, *30*, No. 2002529.
- (24) Kubo, T.; Häusermann, R.; Tsurumi, J.; Soeda, J.; Okada, Y.; Yamashita, Y.; Akamatsu, N.; Shishido, A.; Mitsui, C.; Okamoto, T.; et al. Suppressing Molecular Vibrations in Organic Semiconductors by Inducing Strain. *Nat. Commun.* **2016**, *7*, No. 11156.
- (25) Lee, M. L.; Fitzgerald, E. A.; Bulsara, M. T.; Currie, M. T.; Lochtefeld, A. Strained Si, Sige, and Ge Channels for High-Mobility Metal-Oxide-Semiconductor Field-Effect Transistors. *J. Appl. Phys.* **2005**, *97*, No. 011101.
- (26) Maiti, R.; Patil, C.; Saadi, M.; Xie, T.; Azadani, J.; Uluutku, B.; Amin, R.; Briggs, A.; Miscuglio, M.; Van Thourhout, D.; et al. et al. Strain-Engineered High-Responsivity MoTe<sub>2</sub> Photodetector for Silicon Photonic Integrated Circuits. *Nat. Photonics* **2020**, *14*, 578–584
- (27) Hou, W.; Azizimanesh, A.; Sewaket, A.; Peña, T.; Watson, C.; Liu, M.; Askari, H.; Wu, S. M. Strain-Based Room-Temperature Non-Volatile Mote 2 Ferroelectric Phase Change Transistor. *Nat. Nanotechnol.* **2019**, *14*, 668–673.
- (28) Carrascoso, F.; Li, H.; Frisenda, R.; Castellanos-Gomez, A. Strain Engineering in Single-, Bi-and Tri-Layer MoS<sub>2</sub>, MoSe<sub>2</sub>, WS<sub>2</sub> and WSe<sub>2</sub>. *Nano Res.* **2021**, *14*, 1698–1703.
- (29) Li, X.; Luo, Y.; Holt, M. V.; Cai, Z.; Fenning, D. P. Residual Nanoscale Strain in Cesium Lead Bromide Perovskite Reduces Stability and Shifts Local Luminescence. *Chem. Mater.* **2019**, *31*, 2778–2785.
- (30) Niehues, I.; Schmidt, R.; Drüppel, M.; Marauhn, P.; Christiansen, D.; Selig, M.; Berghäuser, G.; Wigger, D.; Schneider, R.; Braasch, L.; et al.et al. Strain Control of Exciton—Phonon Coupling in Atomically Thin Semiconductors. *Nano Lett.* **2018**, *18*, 1751–1757.
- (31) Wang, Y.; Cong, C.; Yang, W.; Shang, J.; Peimyoo, N.; Chen, Y.; Kang, J.; Wang, J.; Huang, W.; Yu, T. Strain-Induced Direct—

- Indirect Bandgap Transition and Phonon Modulation in Monolayer WS<sub>2</sub>. Nano Res. **2015**, 8, 2562-2572.
- (32) Conley, H. J.; Wang, B.; Ziegler, J. I.; Haglund, R. F., Jr; Pantelides, S. T.; Bolotin, K. I. Bandgap Engineering of Strained Monolayer and Bilayer MoS<sub>2</sub>. Nano Lett. 2013, 13, 3626-3630.
- (33) Hui, Y. Y.; Liu, X.; Jie, W.; Chan, N. Y.; Hao, J.; Hsu, Y.-T.; Li, L.-J.; Guo, W.; Lau, S. P. Exceptional Tunability of Band Energy in a Compressively Strained Trilayer MoS<sub>2</sub> Sheet. ACS Nano 2013, 7, 7126-7131.
- (34) Sekitani, T.; Someya, T. Stretchable, Large-Area Organic Electronics. Adv. Mater. 2010, 22, 2228-2246.
- (35) Lipomi, D. J.; Tee, B. C. K.; Vosgueritchian, M.; Bao, Z. Stretchable Organic Solar Cells. Adv. Mater. 2011, 23, 1771-1775.
- (36) da Silva Filho, D. A.; Kim, E. G.; Brédas, J. L. Transport Properties in the Rubrene Crystal: Electronic Coupling and Vibrational Reorganization Energy. Adv. Mater. 2005, 17, 1072-1076.
- (37) Fornari, R. P.; Aragó, J.; Troisi, A. Exciton Dynamics in Phthalocyanine Molecular Crystals. J. Phys. Chem. C 2016, 120, 7987-7996.
- (38) Fratini, S.; Ciuchi, S.; Mayou, D.; De Laissardière, G. T.; Troisi, A. A Map of High-Mobility Molecular Semiconductors. Nat. Mater. 2017, 16, 998-1002.
- (39) Ortmann, F.; Bechstedt, F.; Hannewald, K. Charge Transport in Organic Crystals: Theory and Modelling. Phys. Status Solidi B 2011, 248, 511-525.
- (40) Popescu, A.; Younts, R. A.; Hoffman, B.; McAfee, T.; Dougherty, D. B.; Ade, H. W.; Gundogdu, K.; Bondarev, I. V. Monitoring Charge Separation Processes in Quasi-One-Dimensional Organic Crystalline Structures. Nano Lett. 2017, 17, 6056-6061.
- (41) Spano, F. C. The Spectral Signatures of Frenkel Polarons in Hand J-Aggregates. Acc. Chem. Res. 2010, 43, 429-439.
- (42) Rawat, N.; Pan, Z.; Manning, L. W.; Lamarche, C. J.; Cour, I.; Headrick, R. L.; Waterman, R.; Woll, A. R.; Furis, M. I. Macroscopic Molecular Ordering and Exciton Delocalization in Crystalline Phthalocyanine Thin Films. J. Phys. Chem. lett. 2015, 6, 1834-1840.
- (43) Yamagata, H.; Spano, F. C. Strong Photophysical Similarities between Conjugated Polymers and J-Aggregates. J. Phys. Chem. Lett. 2014, 5, 622-632.
- (44) Song, C.; Fan, F.; Xuan, N.; Huang, S.; Zhang, G.; Wang, C.; Sun, Z.; Wu, H.; Yan, H. Largely Tunable Band Structures of Few-Layer InSe by Uniaxial Strain. ACS Appl. Mater. Interfaces 2018, 10, 3994-4000.
- (45) Manning, L. W.; Rawat, N.; Lamarche, C.; Waterman, R.; Headrick, R. L.; Furis, M. Exciton Delocalization in H<sub>2</sub>OBPc<sub>1-x</sub>MOBPc<sub>x</sub> (M= Co, Cu, Ni, Mn) Crystalline Thin-Film Organic Alloys. J. Phys. Chem. C 2016, 120, 11966-11976.
- (46) Pan, Z.; Rawat, N.; Cour, I.; Manning, L.; Headrick, R.; Furis, M. Polarization-Resolved Spectroscopy Imaging of Grain Boundaries and Optical Excitations in Crystalline Organic Thin Films. Nat. Commun. 2015, 6, No. 8201.
- (47) Liang, L.; Burrill, K.; Furis, M. I. Transition Dipole Moments of One-Dimensional Excitons in Soluble Phthalocyanine Thin Films. J. Phys. Chem. C 2021, 125, 27966-27974.
- (48) Gao, Y.; Chen, Y.; Li, R.; Bian, Y.; Li, X.; Jiang, J. Nonperipherally Octa (Butyloxy)-Substituted Phthalocyanine Derivatives with Good Crystallinity: Effects of Metal-Ligand Coordination on the Molecular Structure, Internal Structure, and Dimensions of Self-Assembled Nanostructures. Chem.-Eur. J. 2009, 15, 13241-
- (49) Basova, T. V.; Kiselev, V. G.; Schuster, B. E.; Peisert, H.; Chasse, T. Experimental and Theoretical Investigation of Vibrational Spectra of Copper Phthalocyanine: Polarized Single-Crystal Raman Spectra, Isotope Effect and DFT Calculations. J. Raman Spectrosc. **2009**, 40, 2080–2087.
- (50) Liu, Z.; Zhang, X.; Zhang, Y.; Jiang, J. Theoretical Investigation of the Molecular, Electronic Structures and Vibrational Spectra of a Series of First Transition Metal Phthalocyanines. Spectrochim. Acta A **2007**, 67, 1232–1246.

- (51) Zhang, X.; Zhang, Y.; Jiang, J. Towards Clarifying the N-M Vibrational Nature of Metallo-Phthalocyanines: Infrared Spectrum of Phthalocyanine Magnesium Complex: Density Functional Calculations. Spectrochim. Acta A 2004, 60, 2195-2200.
- (52) Aroca, R.; Dilella, D. P.; Loutfy, R. O. Raman Spectra of Solid Films—I: Metal-Free Phthalocyanine. J. Phys. Chem. Solids 1982, 43,
- (53) Sosorev, A. Y.; Maslennikov, D. R.; Kharlanov, O. G.; Chernyshov, I. Y.; Bruevich, V. V.; Paraschuk, D. Y. Impact of Low-Frequency Vibrations on Charge Transport in High-Mobility Organic Semiconductors. Phys. Status Solidi RRL 2019, 13, No. 1970016.
- (54) Zallen, R. Pressure-Raman Effects and Vibrational Scaling Laws in Molecular Crystals: S 8 and as 2 S 3. Phys. Rev. B 1974, 9, No. 4485.
- (55) Abadias, G.; Chason, E.; Keckes, J.; Sebastiani, M.; Thompson, G. B.; Barthel, E.; Doll, G. L.; Murray, C. E.; Stoessel, C. H.; Martinu, L. Stress in Thin Films and Coatings: Current Status, Challenges, and Prospects. J. Vac. Sci. Technol. A 2018, 36, No. 020801.
- (56) Lessard, B. H.; White, R. T.; Al-Amar, M.; Plint, T.; Castrucci, J. S.; Josey, D. S.; Lu, Z.-H.; Bender, T. P. Assessing the Potential Roles of Silicon and Germanium Phthalocyanines in Planar Heterojunction Organic Photovoltaic Devices and How Pentafluoro Phenoxylation Can Enhance Π-Π Interactions and Device Performance. ACS Appl. Mater. Interfaces 2015, 7, 5076-5088.
- (57) Melville, O. A.; Lessard, B. H.; Bender, T. P. Phthalocyanine-Based Organic Thin-Film Transistors: A Review of Recent Advances. ACS Appl. Mater. Interfaces 2015, 7, 13105-13118.
- (58) Lessard, B. H.; Dang, J. D.; Grant, T. M.; Gao, D.; Seferos, D. S.; Bender, T. P. Bis (Tri-N-Hexylsilyl Oxide) Silicon Phthalocyanine: A Unique Additive in Ternary Bulk Heterojunction Organic Photovoltaic Devices. ACS Appl. Mater. Interfaces 2014, 6, 15040-

# **□** Recommended by ACS

# Photon Upconversion in a Vapor Deposited 2D **Inorganic-Organic Semiconductor Heterostructure**

Reynolds Dziobek-Garrett, Thomas J. Kempa, et al.

MAY 16, 2023 NANO LETTERS

READ 2

# Threshold-like Superlinear Accumulation of Excitons in a **Gated Monolayer Transition Metal Dichalcogenide**

Zhen Wang, Cun-Zheng Ning, et al.

JANUARY 09, 2023 ACS PHOTONICS

READ **C** 

## **Enhancing the Purity of Deterministically Placed Quantum** Emitters in Monolayer WSe,

Christopher E. Stevens, Joshua R. Hendrickson, et al.

NOVEMBER 29, 2022

ACS NANO

READ **C** 

# "Dead" Exciton Layer and Exciton Anisotropy of Bulk MoS<sub>2</sub> **Extracted from Optical Measurements**

Vasyl G. Kravets, Alexander N. Grigorenko, et al.

NOVEMBER 09, 2022

ACS NANO

READ 2

Get More Suggestions >